Now the Rollin film is of the order of 100 molecular layers thick, and it forms over available surfaces quite suddenly as the temperature is lowered past the λ-point. In the outer edges of the Rollin film the liquid must be in nearly the same state as bulk liquid. This does not say, however, that the superfluid cannot be in a somewhat different condition near the wall, and for a greater distance than the natural thickness of the film *above* the λ-point; in fact, the peculiar ability of the superfluid to stabilize so thick a film would imply that this must be the case. If it is true that $\bar{S}_2 \neq 0$, and still London's equation holds, then it must follow on the basis of the above picture, that the partial molal entropy of the superfluid near the wall must be zero (and its enthalpy must have the proper value for it to exist in equilibrium) and the superflow must take place in these layers. One might question the hypothesis, and feel that it is easier to believe from the experimental check of London's equation simply that $\bar{S}_2$ is equal to zero for bulk liquid as well as for layers near the wall of the tube. However, the thermomechanical effect alone cannot prove this, and the discussion of the effect of He^3 on the λ-point does offer some, at least circumstantial evidence, that $\bar{S}_2$ may not be zero.[20]

In conclusion we should call attention once more to the tentative character of the very mechanistic approach used in this section. Gorter's equation appears to rest necessarily on some such mechanistic approach with, in addition, some such special assumptions as we have indicated. London's equation, on the other hand, can be based upon a much more general type of deduction and related directly to a quantity like c which can be, at least in principle, experimentally determined.

Without committing them to any of the views expressed in this paper, I wish to thank Professor S. R. de Groot and Dr. K. G. Denbigh for stimulating discussions.

[20] J. C. Morrow, Phys. Rev. 84, 502 (1951).

PHYSICAL REVIEW VOLUME 89, NUMBER 4 FEBRUARY 15, 1953

Field Emission: Large Current Densities, Space Charge, and the Vacuum Arc*,†

W. P. Dyke and J. K. Trolan
Physics Department, Linfield College, McMinnville, Oregon

(Received October 16, 1952)

Field emission was obtained from a single crystal tungsten emitter under conditions of very high vacuum and clean surfaces. The geometry of the emitter was determined by electron microscopy permitting accurate calculation of both the surface electric field and an average current density. The use of pulse electronic techniques extended the observations to the upper limit of the current densities for which the normal field emission was stable. Above this limit an explosive vacuum arc occurred between electrodes.

From these experiments the following conclusions were drawn. (1) The wave mechanical, image force corrected theory quantitatively predicted the observed average current density up to that density for which space charge dominated the emission. (2) Space charge was effective at a current density of the order of 10^7 amperes/cm², where a marked deviation occurred from the usual current-voltage relationship. Space charge effects permitted the simultaneous operation of multiple emitting areas of differing geometries. (3) At a still higher critical current density in the range 10^7 to 10^8 amperes/cm², a field emission initiated vacuum arc occurred between electrodes resulting in a change of emitter geometry. Current density was the dominant criterion for the initiation of the vacuum arc.

THE field emission of electrons from a cold metallic cathode occurs in the presence of a large surface electric field. Observations on the effect were published by Lilienfeld[1] in 1922 following the initial report of Wood;[2] later, Millikan and Lauritsen[3] introduced the following empirical relationship describing the phenomena:

$$I = C \exp(-B/V), \tag{1}$$

where I and V are current and voltage, respectively, and C and B are constants.

Classical theory[4] fails completely to provide a field emission mechanism. According to wave mechanics, which has been applied with increasing success, the copious conduction electrons penetrate the potential barrier at the metallic surface when the barrier is thinned by the applied field. Comparisons between experiment and the original theory of Fowler and Nordheim,[5] which assumed a simple triangular poten-

* This work was supported by the Research Corporation, the U. S. Office of Naval Research and Linfield College; additional support during the later part of the work was received from the Microwave Laboratory of the University of California.

† Preliminary reports on this work were given at several meetings of the Division of Electron Physics of the American Physical Society: Phys. Rev. **82**, 575 (1951); **85**, 391 (1952); **85**, 752 (1952). As partial fulfillment for the Ph.D. degree, preliminary data to part of this work was submitted to the Physics Department, Oregon State College by the second author.

[1] J. E. Lilienfeld, Physik. Z. **23**, 506 (1922).

[2] R. W. Wood, Phys. Rev. **5**, 1 (1897).

[3] R. A. Millikan and C. C. Lauritsen, Proc. Natl. Acad. Sci. U. S. **14**, 1 (1928).

[4] W. Schottky, Z. Physik **14**, 80 (1923).

[5] R. H. Fowler and L. W. Nordheim, Proc. Roy. Soc. (London) **A119**, 173 (1928).

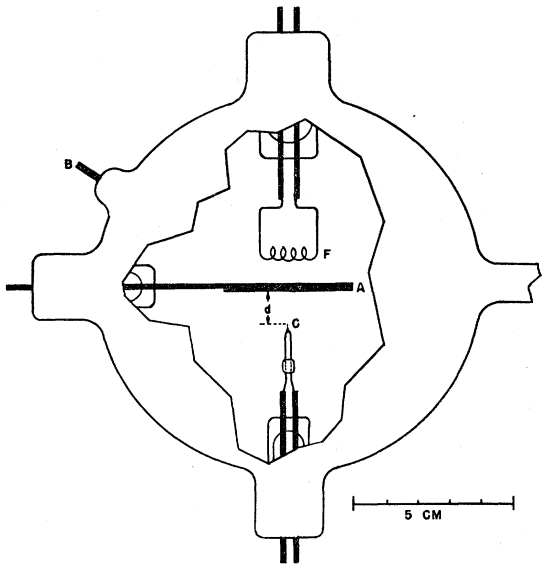

FIG. 1. Experimental field emission tube.

tial barrier, have been well summarized by Jenkins.[6]

When the theory[5] is modified to include the effect of the electron image force,[7] there results the relationship[8]

$$J=1.55\times10^{-6}\frac{F^2}{\phi}\exp\left[\frac{-6.85\times10^{7}\phi^{\frac{3}{2}}f(y)}{F}\right], \quad (2)$$

where J is the current density in amperes/cm^2, F is the electric field in volts/cm, ϕ is the work function in electron volts, and $f(y)$ is an elliptic function of the variable

$$y=3.78\times10^{-4}F^{\frac{1}{2}}/\phi.$$

Values of $f(y)$ are available in tabular[7] or graphic[9] form.

Early comparisons between experiment and theory were limited by the inability to resolve field emitter geometries by use of optical microscopy. Haefer[10] improved the resolution of the emitter geometry by use of electron microscopy and verified Eq. (2) within a rather large experimental error, which was due to the use of an approximate electric field calculation[11] and the inability to view the emission pattern[12] and hence to judge the surface cleanliness while the current-voltage relationship was observed. Current densities up to 10^6 amperes/cm^2 were recorded for the steady state emission to which observations were limited.

Since the theory (2) predicts current densities in excess of 10^{10} amperes/cm^2, which is considerably greater than those reported previously[10] by direct current methods, it is of interest to extend the comparison between experiment and theory by the use of suitable pulse electronic techniques with which improved cathode stability would be expected, since positive ion bombardment, resistive heating, surface contamination, migration, etc., are thus minimized.

The predicted field current densities are sufficiently large to stimulate interest in the practical application of field emission and to support its proposed contribution to voltage breakdown in vacuum. It was therefore desirable that the experimental observations include the upper limit of current densities for which the normal field emission was stable at microsecond pulse lengths and those densities above which voltage breakdown occurred between electrodes.

EXPERIMENTAL METHOD

The experimental tube envelope (Fig. 1), which was Pyrex, enclosed a needle shaped tungsten field emission cathode (C) which faced the anode (A) a sheet of 5-mil molybdenum, with an anode-cathode spacing $d=0.5$ cm. Electrons from the filament F were used to heat the anode by bombardment during the outgassing procedure.

A thin aluminum coating was evaporated onto the interior of the glass envelope of the experimental tube and connected electrically to the inseal B. It was held at anode potential in order to prevent the glass envelope from charging electrically. It has been found impossible to obtain reliable, reproducible data when uncoated envelopes of the same type were used.

The present anode structure was chosen to inhibit cathode contamination and voltage breakdown due to anode effects when large field currents were emitted. The anode was outgassed, cleaned, and smoothed at high temperature to minimize the bombardment of the cathode by anode material, ions, or clusters. The cathode surface was known to be clean and smooth (prior to breakdown) judged from electron micrographs, electrical behavior, and from the operation of numerous similar cathodes in preliminary experiments in which the emission pattern was viewed on metal backed phosphor anode screens. Suitable techniques for emitter fabrication, conditioning, and high vacuum were thus chosen;[11] however, metal backed phosphor anodes, which were not readily outgassed, contributed excessive cathode contamination when the emitted direct current was large, and were thus not suited to the present experiments.

The field emission cathode was electrolytically etched from a blank of commercial 5-mil tungsten wire (Callite 200H) mounted at the apex of a hairpin filament which was used to outgas and smooth the emitter.[11]

The experimental tube was evacuated with a type GHG-10-02 D.P.I. mercury diffusion pump and liquid air traps. The high vacuum side of the system was baked at 500°C, after which all metal parts (except the

[6] R. O. Jenkins, *Reports on Progress in Physics* (The Physical Society, London, 1943), Vol. IX, p. 177.
[7] L. W. Nordheim, Proc. Roy. Soc. (London) **A121**, 626 (1928).
[8] A. Sommerfeld and H. Bethe, *Handbuch der Physik* (J. Springer, Berlin, 1933), Vol. XXIV, No. 2, p. 441.
[9] F. R. Abbott and J. E. Henderson, Phys. Rev. **56**, 113 (1939).
[10] R. H. Haefer, Z. Physik **116**, 604 (1940).
[11] Dyke, Trolan, and Dolan (to be published).
[12] E. W. Mueller, Z. Physik **106**, 541 (1937).

coating B) were outgassed simultaneously at a temperature above which evaporation was appreciable. After a minimum of four such cycles, the experimental tube, a Bayard-Alpert ionization gauge,[13] and a separate Pyrex envelope housing a tantalum getter filament were sealed off as a unit at a pressure of 10^{-9} mm of Hg or better as indicated by the gauge. Subsequently, a layer of tantalum was evaporated onto the wall of the getter tube, after which all metal parts of the experimental tube were again heated. Residual gas was thus transferred to the active tantalum layer, and after several such cycles the pressure of chemically active gases was reduced to 10^{-12} mm of Hg or better, judged by the contamination rate of the field emission cathode.[14] The final vacuum was thus sufficiently good to insure that the electrode surfaces remained free from contamination by residual gases for a time that was long compared with that needed for the experiment, i.e., several hours.

Under these conditions it was possible to draw stable direct currents up to 8 milliamperes at 20 kv, corresponding to a cathode current density of the order to 10^6 amperes/cm^2 as will be shown later. Although the cathode would probably emit larger stable direct currents, the 8-milliampere current limitation was imposed to avoid excessive anode temperature which accelerates the contamination process. At this level the contamination of the cathode surface was evidenced by a decrease in direct current over a period of seconds, the cathode returning to its initial condition following a flash at 2200°C for a few seconds in the absence of field. The contaminant was probably oxygen[12] liberated at the anode, whose temperature exceeded 1000°C at the current and voltage levels indicated above. Pulsed currents considerably larger than those achieved with direct current techniques were drawn without evidence of cathode contamination.

Figure 2 describes the experimental system. Potentials in the range 0–20 kv were furnished by a rectified 800-cycle power supply whose input was regulated mechanically by the inertia of a motor-generator set. During direct current operation, potentials were read by a Weston Model 622 milliammeter in series with a 20-megohm Weston Type 2 resistor. Currents were indicated by a current sensitive Leeds & Northrup Type R galvanometer.

During pulsed operation, a positive potential which approximated a square wave of either $\frac{1}{2}$ or 2 microsecond duration and whose amplitude was variable from 2 to 35 kv was furnished by a pulse generator which included a conventional 4 section, 6.7 ohm line (for 2 μsec operation) or a 50-ohm coaxial cable (for $\frac{1}{2}$ μsec operation) either of whose outputs (8 kv or less) was switched by a triggered spark gap directly to the experimental tube or to the primary of a pulse transformer (T807, AN/APS-3). Its output potential, which was applied directly to the anode of the experimental tube, was divided by a conventional calibrated capacity divider[15] whose output was connected to the deflection plates of a Tektronix Type 511 oscilloscope (CRT_1). A Fairchild Type A, 35 mm f/2.3 automatic camera (C_1) recorded the current which was drawn by the experimental tube. For this purpose, a noninductive carbon resistance was inserted between the cathode and ground and was connected at the cathode end directly to the deflection plates of CRT_2. A Tektronix 517 oscilloscope was used to record the current in the latter part of the work.

Pulsed data were taken on a single-shot basis. A key activated the trigger generator, Fig. 2, whose voltage impulse caused the system to cycle once and then return to the quiescent state. It simultaneously triggered the pulse generator and the sweeps of both oscilloscopes and opened the shutters of the cameras (C_1) and (C_2) and advanced their films. Filament temperatures were measured with a Leeds & Northrup optical pyrometer.

A Sorenson voltage regulator stabilized the primary supply for both oscilloscopes.

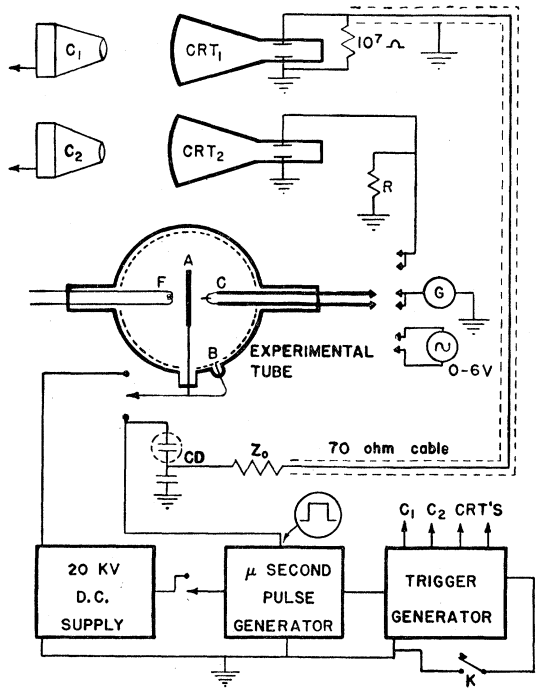

FIG. 2. Experimental electronic circuit used for both pulse and direct current measurements. C—camera; CRT—oscilloscope; G—galvanometer; CD—capacity divider.

[13] R. T. Bayard and D. Alpert, Rev. Sci. Instr. **21**, 6, 571 (1950).

[14] J. A. Becker, Report Eleventh Annual Conference on Physical Electronics, Massachusetts Institute of Technology, 1951 (unpublished).

[15] G. N. Glasoe and J. V. Le Bacqz, *Pulse Generators* (McGraw-Hill Book Company, Inc., New York, 1948), Radiation Laboratory Series.

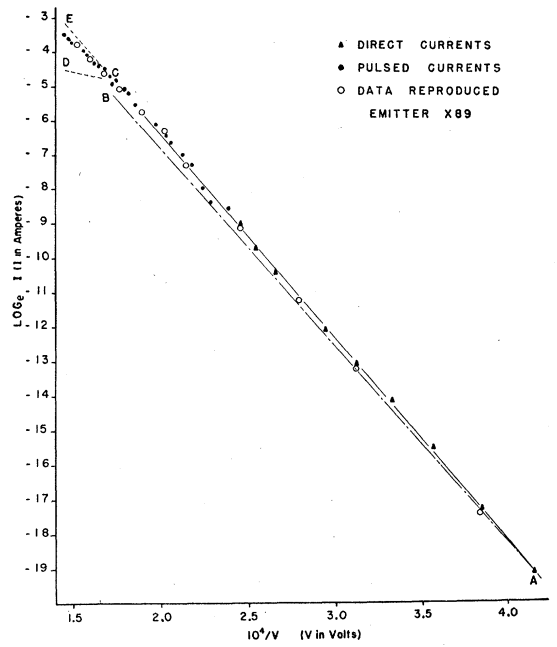

FIG. 3. Field current-voltage characteristic for combined pulse and direct current operation of emitter X-89. Curve AB represents the characteristic for the hypothetical case of a constant emitting area equal to that at A. Curve CE was predicted by the theory (2) and curve CD from $J \propto V^{\frac{1}{2}}$, both assuming a uniform distribution of current density and a constant emitting area.

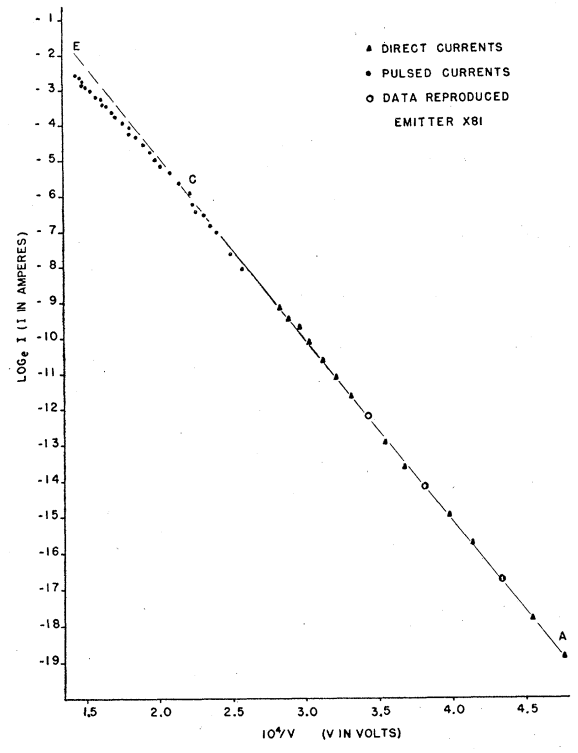

FIG. 4. Field current-voltage characteristic for combined pulse and direct current operation of emitter X-81.

EXPERIMENTAL RESULTS

The current-voltage relationships for emitters X-89, X-81, N-10, and Q-7 for combined direct current and pulsed operations are shown in Figs. 3, 4, 5, and 6, respectively.

Figure 3 illustrates the typical experimental procedure. Direct current readings were taken, then repeated (not shown). Pulsed currents of 1 μsec duration were then drawn, immediately following which the data were reproduced in the sense of decreasing currents, the reproducibility precluding the possibility of significant

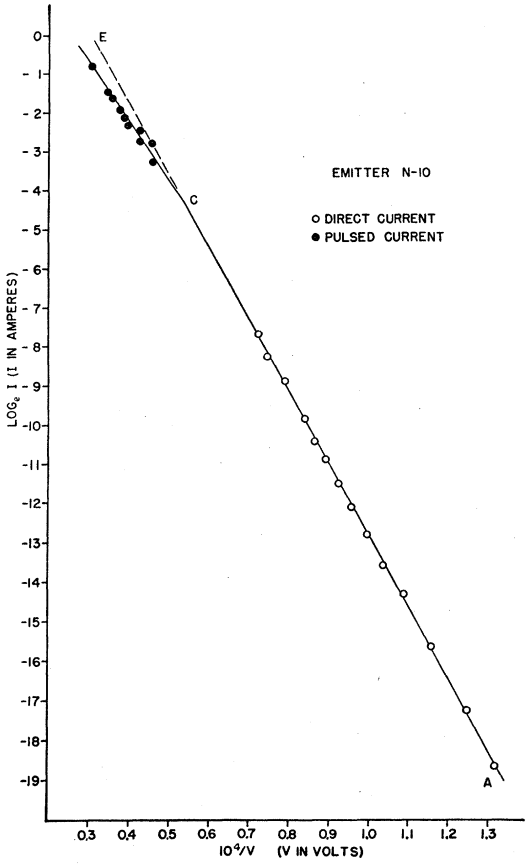

FIG. 5. Field current-voltage characteristic for combined pulse and direct current operation of emitter N-10.

cathode contamination or geometric alteration during the experiments.

The current-voltage relationships in Figs. 3, 4, 5, and 6 have several characteristics in common.

1. Each graph is linear for a considerable range of currents (A to C) below a critical current I_C, in which range the empirical equation (1) was confirmed.

2. At currents greater than I_c the current-voltage relationships depart from linearity in the direction of lower current for a given voltage, the departure presumably being due to space charge, since cathode contamination or geometric alteration are precluded by the reproducibility of the data.

3. At voltages slightly higher than the maximum value shown on each graph the normal field emission was abruptly terminated

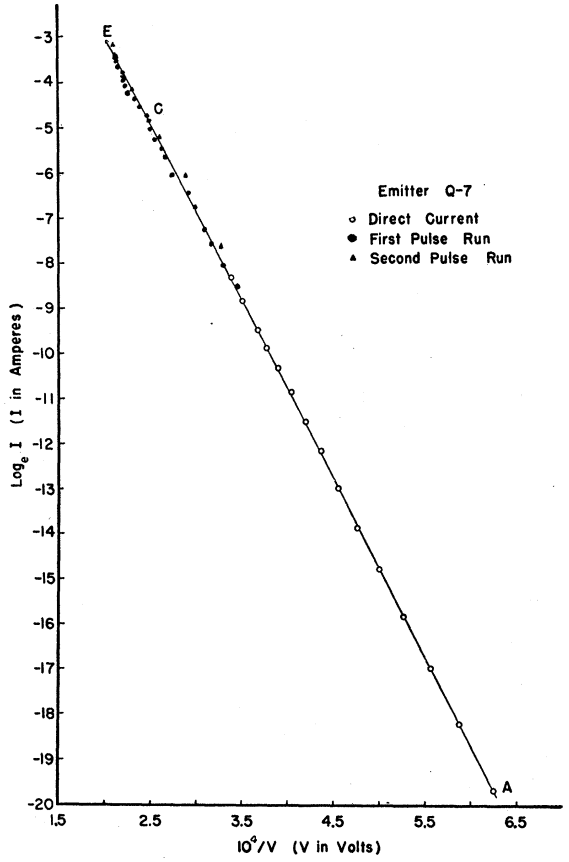

FIG. 6. Field current-voltage characteristic for combined pulse and direct current operation of emitter Q-7.

by a low impedance vacuum arc (except for emitter X-89). While the pulsed field emission was stable at current densities a factor of two or more lower than the arc level, the emitter tip was usually damaged (melted) during the arc.

The emission from X-89 was discontinued at a current level slightly below that for which an arc was expected, and the emitter was removed from the experimental tube in order to obtain the electron micrographs of two profiles of the emitter shown in Fig. 7.

Electron micrographs of two profiles of emitter N-10 are shown in Fig. 8A, prior to insertion into the experimental tube (the radius of this emitter was later increased slightly by surface migration at high temperature during the final outgassing procedure, judged from its subsequent electrical behavior). After arc damage this emitter appeared as in Fig. 8B, which is a composite of several electron micrographs. Figure 9 shows a typical profile of emitter Q-7 after arc damage.

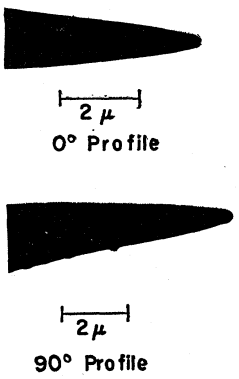

FIG. 7. Electron micrographs of two profiles of emitter X-89 following its experimental use as a field emitter.

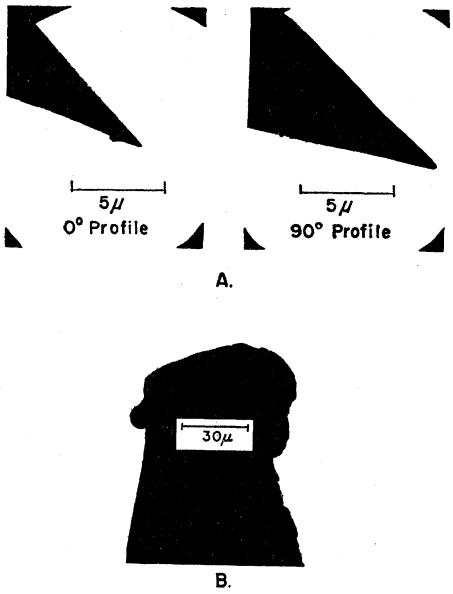

FIG. 8. A. Electron micrographs of two profiles of emitter X-89 prior to its insertion into the experimental tube; B. a composite of several electron micrographs showing one profile of emitter N-10 after a vacuum arc.

RESULTS

The analysis of the present experimental data (I) over most of its range further supports the validity of the wave mechanical, field emission theory involving the electron image force and extends its comparison with experiment to higher current densities than those previously reported, (II) presents evidence for the presence of space charge limited field emission, and (III) suggests mechanisms which may have initiated the voltage breakdown leading to the vacuum arc. This analysis follows.

I. Comparison between Experiment and Theory

A current density $\bar{J}$, an average for the emitting area A, was derived from the present data and com-

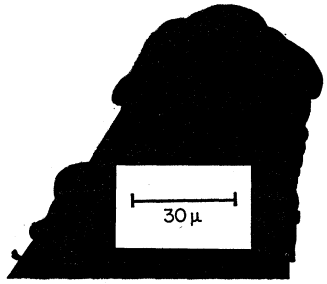

FIG. 9. A composite of several electron micrographs showing one profile of emitter Q-7 after vacuum arc.

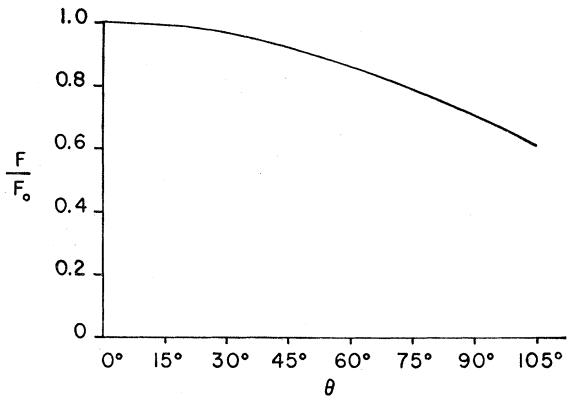

FIG. 10. The dependence of electric field F upon polar angle θ for emitter X-89 calculated with use of an equipotential surface which was closely fitted to the emitter profile judged from its electron micrographs ($\theta=0°$, $F=F_0$ at the apex).

pared with the current density J predicted by the theory (2) when the electric field F_0 at the emitter apex and the value $\bar{\phi}=4.5$ ev were used. When A was known, values of $\bar{J}$ were readily calculated from

$$\bar{J}=I/A, \tag{3}$$

where I was the experimental current.

For emitter X-89, the emitting area was estimated from the measured emitter radius and the calculated dependence of current density on polar angle θ, measured from the emitter apex. For this emitter, whose geometry was determined from electron micrographs (Fig. 7) the ratio F/F_0 as a function of θ calculated by a previous method[11] is shown in Fig. 10. This, with the theory (2) and $\phi=4.5$ ev, predicted the ratio J/J_0 as a function of θ shown in Fig. 11. Curve C resulted from $F_0=7\times10^7$ volts/cm, curve A from $F_0=3\times10^7$ volts/cm, these two values of F_0 corresponding to the points C and A on the graph of Fig. 3, i.e., to the extremities of its linear portion, as will be shown.

Eighty-five percent of the total current was emitted by the area bounded by $\theta=53°$ for the curve C and $\theta=40°$ for curve A (Fig. 11). An extension of these boundaries to larger values of θ would result in an unreasonable increase in area without significant current increase. With the emission boundary thus arbitrarily defined, and with the emitter radius $r=2.3\times10^{-5}$ cm, averaged from the two micrographs of Fig. 7, the areas corresponding to C and A are $A_C=1.2\times10^{-9}$ cm², $A_A=7.6\times10^{-10}$ cm². These, with Eq. (3) and currents at C and A from Fig. 3, yielded current densities $\bar{J}_C=6\times10^6$ amperes/cm², and $\bar{J}_A=6$ amperes/cm². This part of the data was readily compared with the theory (2), as follows.

The electric field F_0 at the emitter apex was calculated from

$$F_0=\beta_0 V, \tag{4}$$

where V was the measured value of the applied potential.

The geometric factor β_0, calculated for emitter X-89 using Eq. (3) of reference 11 with $a=0.33\times10^{-5}$ cm, $r_0=1.8\times10^{-5}$ cm, and $n=0.07$, was

$$\beta_0=(9.9\pm1.5)\times10^3 \text{ cm}^{-1}. \tag{5}$$

The significant experimental errors in β_0 occurred in the calibration of the electron microscope (10 percent) and the determination of emitter geometry averaged from the electron micrographs of its several profiles (5 percent).

Equation (5) includes a 7 percent correction to account for the effect of the supporting filament structure.[16] No significant correction was required for the effect on β_0 introduced by the difference between the experimental anode (Fig. 1) and the theoretical anode used for the calculation of β_0 [reference 11, Eq. (2)] since the effect was necessarily small compared to the 10 percent change in β_0 noticed when the aluminum coating on the inner surface of the envelope of the experimental tube (Fig. 1) was changed from anode potential to emitter potential. This value of β_0 agrees within the experimental error with the value β_m which the theory (2) required in order to predict the observed experimental current-voltage curve. Use of Eqs. (2) and (3) with the assumptions of a uniform work function $\bar{\phi}$ and a constant emitting area A over which the electric field had the constant value F_m gave

$$\beta_m=\left[\frac{d(\ln J)}{d(10^8/F)}\Big/\frac{d(\ln I)}{d(10^4/V)}\right]\times10^4. \tag{6}$$

To evaluate β_m in the present case the theory (2) was

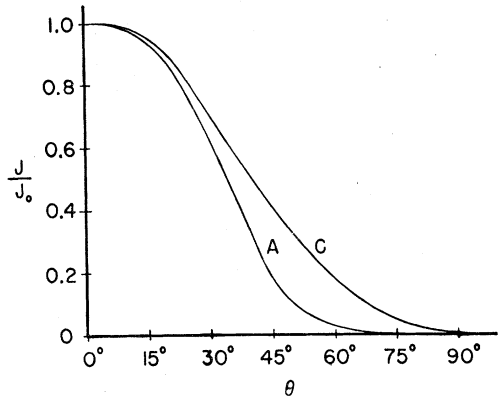

FIG. 11. The dependence of current density J upon polar angle θ (measured from the emitter apex) calculated for emitter X-89 from the field emission theory (2) and the data in Figure 10, assuming a constant work function $\phi=4.5$ ev. Curve A for $F_0=3\times10^7$ volts/cm; curve C for $F_0=7\times10^7$ volts/cm corresponding to the points A and C of Fig. 3.

[16] Emission was obtained from a long, needle-shaped field emitter in another experimental tube, with and without the effect of a typical filament structure which was slid along the needle in the final vacuum with the aid of an external magnet. The filament was moved from its normal position (2 mm from the emitter tip), to another position far removed from the tip. The corresponding change in β_0 was calculated from the change in applied potential required to establish a common current.

TABLE I. Data for several emitters.

A	B	C	D	E	F	G	H	K
Emitter number	β_0 cm^{-1}	β_m cm^{-1}	$\bar{J}_C$ amp/cm^2	$\bar{J}_A$ amp/cm^2	Emitter radius cm	Emitter cone angle in degrees	$\bar{J}_X$ amp/cm^2	V_{max} kv
X-89	9.9×10^3	12.8×10^3	6×10^6	6	2.2×10^{-5}	13	2×10^7	6.9
X-81		14.6×10^3	7×10^6	11	2.7×10^{-5}	10	3×10^7	6.9
N-10		4.0×10^3	9×10^6	6	2.5×10^{-5}	32	2×10^8	32.1
Q-7		19.5×10^3	1×10^7	3×10^2	1.5×10^{-5}	6.5	6×10^7	4.75

graphed in Fig. 12 with $\bar{\phi}=4.5$ ev; the current-voltage relationship AB (Fig. 3) for emitter X-89 was calculated for the required hypothetical case of a constant emitting area with the aid of the data from Fig. 11. According to (6), the ratio of the slopes of these two graphs yield

$$\beta_m=(12.8\pm1.9\times10^3\ \text{cm}^{-1}). \quad (7)$$

The error in β_m due to the ignored variation of F with θ (Fig. 10) was less than 5 percent; that introduced by the neglect of the known distribution of work function with crystallographic direction[17] was less than 7 percent. With other minor errors such as those inherent in the current and voltage measurement, β_m was known within ±15 percent. While β_0 and β_m for emitter X-89 agree within the combined experimental error, additional data from four other emitters indicated that $\beta_m>\beta_0$ by approximately the same percentage in each case.

Careful inspection of the electron micrographs of emitter X-89 revealed that the radius of curvature of the surface near the tip varied slightly with crystallographic direction; apparently the simple crystallographic faces (probably 110) were planes of small but significant area. The surface at other crystallographic directions had smaller than average radii of curvature and hence larger values of β than apparent from (5) and Fig. 10; these surfaces were probably those for which $\phi<\bar{\phi}$ according to Nichols;[17] hence most of the current originated at these surfaces. These effects account at least in part for the observed difference between β_m and β_0, the former being probably more correct than the latter.

This conclusion was strengthened when the experimental current densities $\bar{J}_C$ and $\bar{J}_A$, previously calculated for emitter X-89, were graphed in Fig. 12 at electric field values calculated from the corresponding voltages V_C and V_A from Fig. 3, using β_m from (6). Thus, the theory (2) and experiment agree in the range of current densities $6<\bar{J}<6\times10^6$ amps/cm^2 within the present experimental error.

Haefer[10] used the hyperboloidal approximation to evaluate β_0 in experiments whose agreement with theory appears to be subject to a larger experimental error than that claimed. No mention was made of the uncertainty in β_0 resulting from the use of the hyperboloidal geometry with emitters whose shapes approximated a cone with a hemispherical cap. A hyperboloid tangent to the emitter at the apex can intersect the emitter at only one other polar angle; either the apex of the hyperboloid has a smaller radius than the emitter, or it diverges from the emitter along the shank. β_0 is increased by the former and decreased by the latter, being sensitive to both.[11] With Haefer's formula for β_0, the two surfaces are coincident at $\theta=0°$ and $\theta=10°$, and fortunately the two opposing errors in β_0 are comrable for this fit.

Haefer's formula yields $\beta_0=8.0\times10^3$ cm^{-1} for emitter X-89, a value lower than the present value (5) by 19 percent. This error, if assigned to Haefer's values of β_0, may be compensated for by the previously ignored effect of the filament structure on β_0, which effect is not less than 25 percent judged from the reported filament structure in his work and the present experiments. Further error in Haefer's work may have resulted from surface contamination, since the published emission pattern [his Fig. 12(a)] is not that now generally accepted for clean tungsten[18,19] as was claimed.

Current densities $\bar{J}_C$ and $\bar{J}_A$ for emitters X-81, N-10, and Q-7 are shown in Table I, columns D and E. When

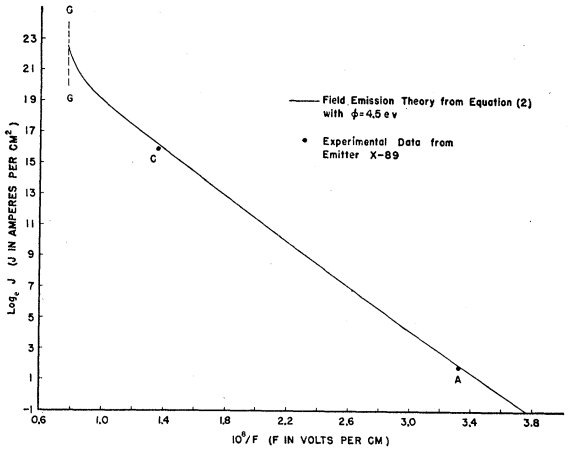

FIG. 12. A graph showing the dependence of current density upon electric field. The solid line resulted from the field emission theory (2) with $\phi=4.5$ ev; the experimental data at A and C represent the average current densities $\bar{J}_A$ and $\bar{J}_C$ with corresponding values of F from $F=\beta_m V$, for emitter X-89. The theory is terminated at the dashed line GG when the surface potential barrier is reduced to the top Fermi electron energy level.

[17] M. H. Nichols, Phys. Rev. **57**, 297 (1940).

[18] E. W. Mueller, Z. Physik **120**, 270 (1943).

[19] J. A. Becker, Bell System Tech. J. **30**, 907 (1951).

the radii of these emitters were obtained from a comparison between the data in Figs. 4, 5, and 6 with the theory (2), current densities were calculated by the method used with emitter X-89. The data from Fig. 11 were assumed applicable to all emitters. This method was used since the required emitter radii were not available from micrographs after use due to arc damage (Figs. 8 and 9); micrographs taken before the emitter was inserted into the experimental tube accurately identified emitter cone angles (Table I, column G) and provided an estimate of emitter radii within a factor of 2 (surface migration caused subsequent changes in radii during the outgassing procedure). Current densities $\bar{J}$ for these three emitters are known within a factor of 3.

The following conclusions were drawn from the foregoing discussion and an inspection of Table I and Figs. 3, 4, 5, 6, and 12: 1. The empirical equation (1) is valid in the range $\bar{J}_A<\bar{J}<\bar{J}_C$ for each emitter. 2. Experimental values of $\bar{J}$ for emitter X-89 agree with those predicted by the theory (2) in the range $6<\bar{J}<6\times10^6$ amps/cm^2, within the experimental error. 3. β_0 and β_m agree within the experimental error; β_0 is sensitive to both emitter radius and cone angle. 4. It is significant that the lowest average current density $\bar{J}_C$ for which space charge effects were observed was of nearly the same value for each emitter; these values of $\bar{J}_C$ were in the range $6\times10^6<\bar{J}_C<1\times10^7$ amperes/cm^2.

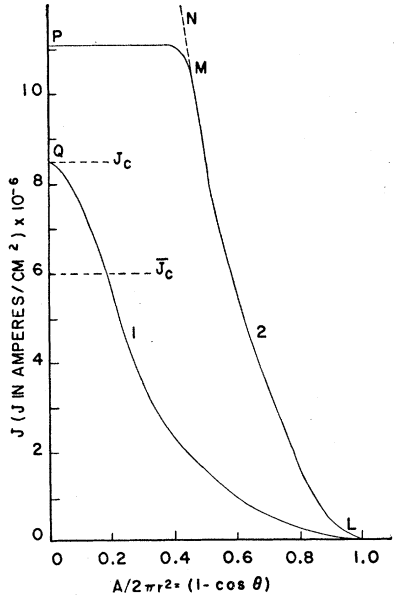

FIG. 13. The surface distribution of current density J for emitter X-89. The abscissas were chosen so that the area under each curve is proportional to the corresponding total current. Curve 1, which is a replot of curve C, Fig. 11, corresponds to the point C, Fig. 3 just prior to the onset of space charge effects ($J=J_C$ at the emitter apex, the average current density being $\bar{J}_C$). Curve 2 corresponds to the largest current shown in Fig. 3, the portion PM resulting from use of Eq. (8) for the space charge limited region, and the portion LM resulting from the use of Eq. (2) for areas in which space charge was absent.

II. Space Charge

It will be shown that space charge necessarily influenced the emission when the current density exceeded a critical value J_C, the effect being confined mainly to the area from which the charge originated provided that J was not considerably greater than J_C. Because the largest value of J was found at the emitter apex where the electric field was greatest (Fig. 11) space charge first influenced the emission from a small area at the apex, the effect spreading to neighboring areas (at larger θ) as the applied voltage was increased sufficiently to increase J to J_C in those regions.

At an area where the emission was space charge limited, i.e., $J\geq J_C$, further increases in current density followed approximately[20]

$$J\propto V^{\frac{3}{2}}, \tag{8}$$

while at areas for which $J<J_C$, the emission increased according to (2). The total observed current increase above I_C (Fig. 3), therefore, fell between the values predicted by (8) (curve CD) and by (2) (curve CE). For both of these limiting curves, a constant emitting area and a uniform current density distribution were assumed; hence, neither of them represents the true experimental situation.

In order to show first that space charge influenced the emission when $J>J_C$, the space charge q_s within a distance $s\ll r$ from a unit emitting area of radius of curvature r was approximated as follows:

The average space charge density $\bar{\rho}_s$ within the distance s was

$$\bar{\rho}_s=J/\bar{v}\ \text{esu/cm}^3, \tag{9}$$

where

$$\bar{v}=\tfrac{1}{2}[v_0+(2e/m)^{\frac{1}{2}}(F_0 s)^{\frac{1}{2}}]\ \text{cm/sec}.$$

The initial velocity v_0 (if any) was negligible. Now,

$$q_s=s\cdot\bar{\rho}_s=2Js^{\frac{1}{2}}(m/2e)^{\frac{1}{2}}F_0^{-\frac{1}{2}} \tag{10}$$

for a unit emitting area. A 1 percent change in β [see Eq. (4)] which was detectable experimentally, would be expected from space charge effects when

$$q_s=0.01\sigma, \tag{11}$$

where σ was the induced surface charge per unit area. Combining (9), (10), and (11) with $\sigma=F_0/4\pi$, $F_0=2.3\times10^5$ esu/cm and $J=3\times10^{16}$ esu/cm^2, the latter two being typical of the experimental data when $V=V_C$, one obtains

$$s=2\times10^{-6}\ \text{cm}. \tag{12}$$

The charge q_s within this distance s from the emitter surface was sufficient to cause a measurable change in the electric field in the proper direction and of sufficient magnitude to account for the departure from linearity observed at the points C of the current-voltage relationships of Figs. 3, 4, 5, and 6. Since s was approxi-

[20] Stern, Gossling, and Fowler, Proc. Roy. Soc. (London) **A124**, 699 (1929).

mately one-tenth of an emitter radius, the charge q_s evidently affected mainly the emission from its area of origin.

Thus, space charge affected only the emission from a small area at the apex of emitter X-89 where $J=J_C$, when $V=V_C$, and the corresponding current-density distribution was that shown in Fig. 11, curve C. These data from curve C were replotted in Fig. 13, curve 1, using values of the variable $A/2\pi r^2=(1-\cos\theta)$ as abscissae (the emitting area being hemispherical), in order that the area under the curve be proportional to the total emission current. During the subsequent voltage increase V_C to V_E (Fig. 3), current densities were assumed to increase in accordance with (8) at areas for which $J>J_C$, and in accordance with (2) at areas for which $J<J_C$. The former required the portion PM of curve 2, (Fig. 13) and the latter gave the portion LM. This interpretation attributes most of the current increase above I_C to an increase in the effective emitting area rather than to a large increase in current density at the emitter apex.

Areas under curves 1 and 2, Fig. 13, are proportional to the respective total currents, their ratio being 2.4. The corresponding ratio of the maximum experimental current $I_{\max}$ to I_C (from Fig. 3) was 3.3. Thus, the present assumptions lead to approximately the observed increase of the total current above I_c for emitter X-89; improved agreement should result when the distribution of ϕ with crystallographic direction[17] is recognized. Such experiments are in progress.

As a result of the effects of space charge, the total emission current from a cathode was increased by the effective operation of emitting areas in parallel at approximately a common current density, although the individual areas had widely different values of current density at lower voltage in the absence of space charge, due to differences in both β_0 and ϕ. This technique was experimentally demonstrated to be valid for multiple emitters.

III. The Field Emission Initiated Vacuum Arc

The foregoing data described the normal behavior of field emitters whose emission was stable and reproducible over a large range of currents extending into the space charge region. It is of particular interest to investigate the phenomena which occurred when attempts were made to extend the emission to still higher currents. When this was done an explosive breakdown occurred between electrodes even under the best initial conditions of vacuum and surface cleanliness, the breakdown phenomena being commonly described as the "vacuum arc." In much of the earlier work with voltage breakdown, the values of the significant variables such as current density, electric field, work function (surface contamination) were uncertain. In the present work these variables were known accurately prior to breakdown.

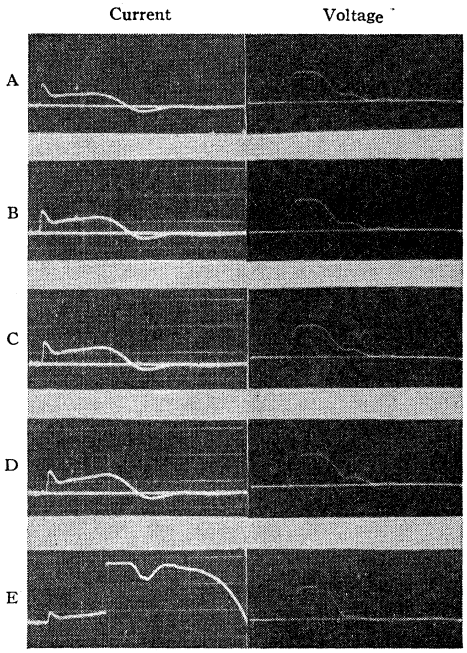

FIG. 14. Current and voltage oscillographs from emitter Q-7 during its transition from the normal field emission (at A) to the vacuum arc (at E) corresponding to a total voltage change of 5 percent. Both current and voltage plateaus are of approximately one microsecond duration. The current oscilloscope sensitivity at E was less by a factor of 2.5 than that at A, B, C, and D.

Breakdown occurred between electrodes when the current density, averaged over the cross-sectional area of the emitter cone at its junction with the emitter hemisphere, exceeded a critical value $\bar{J}_x$; to a good approximation

$$\bar{J}_x=(I_{\max}/\pi r^2)\ \text{amperes/cm}^2, \qquad (7)$$

where $I_{\max}$ was the largest value of the normal, stable field current prior to breakdown shown in the curves of Figs. 4, 5, and 6, and r was the average radius of the emitter hemisphere (Table I, column F). The values of $\bar{J}_x$ from the several emitters (column H) are in sufficient agreement to suggest that current density was the most important variable in the present voltage breakdown; no correlation with voltage was apparent from an inspection of column K.

The current and voltage oscilloscope traces from emitter Q-7 taken during the transition between the normal, stable field emission, Fig. 14A, and the terminating vacuum arc, Fig. 14E, are instructive. The current trace A, for which $I=2.2\times10^{-2}$ ampere, was typical of all smaller currents. It exhibits a constant current plateau of approximately 1 microsecond duration (the anomalies at the leading and trailing edges of the current pulse were characteristic of the cathode circuit and are not related to the emission current). A 4 percent increase in voltage which would normally result in a 25 percent current increase caused the change A to D, marked by a "tilted" current trace

indicating an increase of current with time during a single pulse (with constant voltage), the degree of tilt increasing with current level. The series A–D was reversible and reproducible, the emitter apparently suffering little change in the process as indicated by the similarity between the first and second pulse runs (Fig. 6) made, respectively, before and after several cycles A–D–A (Fig. 14). A one percent increase in voltage yielded the nonreversible change D–E, voltage breakdown occurring near the expected peak of the current pulse. The time of formation of the ensuing vacuum arc was less than 5×10^{-8} sec, judged from an inspection of the current trace E (total current during the arc was greater than that indicated by the current trace E, due to saturation of the oscilloscope amplifier, Tektronix Type 517). Emitter Q-7 appeared as in Fig. 9, after arc, its radius increased by a factor of approximately 150 by a process in which it was melted.

The foregoing data suggest that voltage breakdown resulted from increased emitter temperature due to a current density dependent mechanism accompanying the emission process. Possible mechanisms which might have produced the required heating are resistive heating and the Nottingham mechanism.[21] The former is favored by the sensitive dependence of the breakdown process to current increase indicated in Fig. 14. A solution for the adiabatic case applied to the present emitters showed that resistive heating would yield an excessive emitter temperature rise in a microsecond when $J\geq10^7$ amperes/cm^2. The increase in emitter temperature predicted by the two mechanisms when heat conduction is considered will be presented in a forthcoming paper together with additional experimental evidence.

The foregoing interpretation is reasonable if the thermal component of the emitted current was comparable in magnitude to the normal field current (accounting for the tilted current pulse, Fig. 14D), a result that is expected according to Le Page and Du Bridge,[22] when the surface potential barrier is not large compared with kT (the barrier in the present case was about 1 ev above the top Fermi level[7] when $F_0=8\times10^7$ v/cm. The work of Guth and Mullin[23] concerning electron emission at intermediate electric fields and temperatures adds further support. The required temperature dependent current increase probably originated in part at least at areas whose normal field emission was not space-charge saturated.

During the formation of the vacuum arc (Fig. 14E) the current increased by approximately two orders of magnitude in 5×10^{-8} second, the normal field emission prior to the arc being space-charge limited in part. The observed current increase required either that $\bar{J}$ was considerably greater than $\bar{J}_C$ in which case space charge was necessarily neutralized, or that the effective emitting area was correspondingly increased, or both. The positive ions required by the former may have been supplied by the heated emitter whose surface material was evaporated as ions or as neutral atoms which were ionized near the emitter surface in the high density electron beam. In view of the required rate of ion delivery, the excellence of the present vacuum, and transit time considerations it is unlikely that the present breakdown was initiated by ions[24] or clusters[25] liberated at the anode.

The observed current increase of two orders of magnitude which accompanied the formation of the vacuum arc was certainly sufficient to account for the additional heating required for the geometric deformation shown in Figs. 8B and 9.

The authors express their appreciation to Professor J. E. Henderson of the University of Washington, who suggested the original line of investigation and who has maintained a continued interest throughout this work. Considerable technical assistance was rendered by L. M. Perry and others of the Physics department at Linfield College.

[21] W. B. Nottingham, Phys. Rev. **59**, 907 (1941).
[22] W. R. Le Page and L. A. Du Bridge, Phys. Rev. **58**, 61 (1940).
[23] E. Guth and C. J. Mullin, Phys. Rev. **61**, 339 (1942).
[24] Webster, Van de Graaff, and Trump, J. Appl. Phys. **23**, 264 (1952).
[25] Lawrence Cranberg, J. Appl. Phys. **23**, 518 (1952).

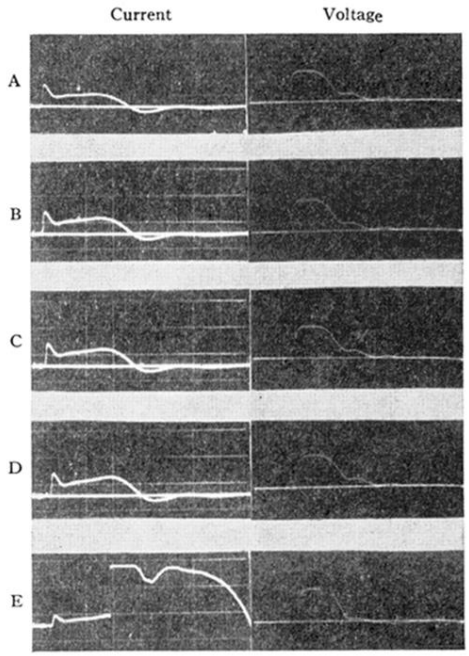

FIG. 14. Current and voltage oscillographs from emitter Q-7 during its transition from the normal field emission (at *A*) to the vacuum arc (at *E*) corresponding to a total voltage change of 5 percent. Both current and voltage plateaus are of approximately one microsecond duration. The current oscilloscope sensitivity at *E* was less by a factor of 2.5 than that at *A*, *B*, *C*, and *D*.